Cell Reports, Volume *42*

Supplemental information

Geometric transformation of cognitive maps for generalization across hippocampal-prefrontal circuits

Wenbo Tang, Justin D. Shin, and Shantanu P. Jadhav

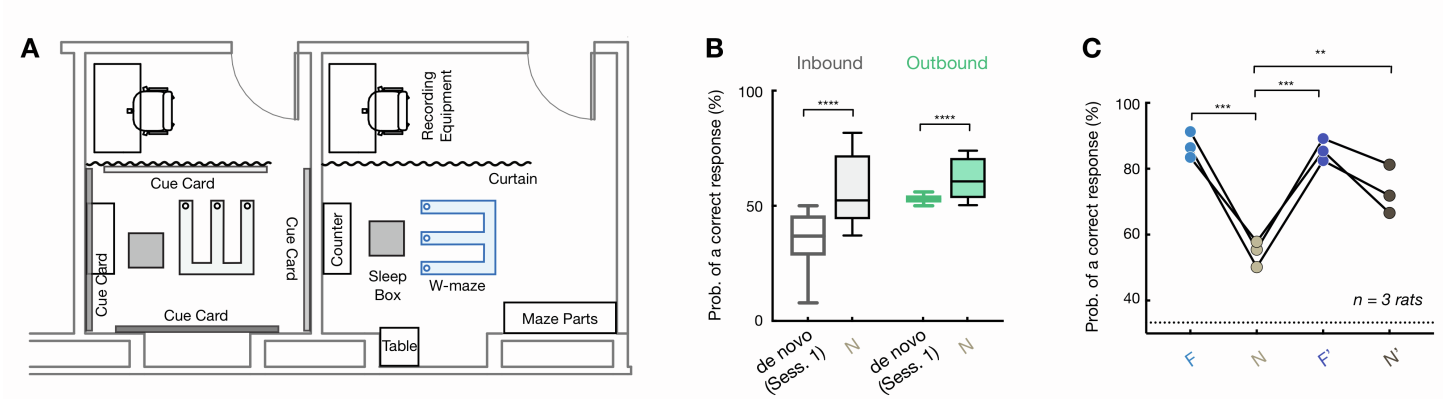

Figure S1. Configuration of recording rooms and memory performance in familiar-novel environments. Related to Figure 1.

(A) Schematic layout of recording rooms for familiar and novel settings. *De novo* learning and F sessions were recorded under the setting in the familiar room (*right*), whereas N and N' sessions were recorded in the novel room (*left*). Each room has a different size and a number of prominent visual cues. Additionally, large cue cards (~4 m^2) with different patterns hung on the walls of the novel room to enhance discriminability.

(B) Proportion correct for inbound (gray) and outbound (green) trials during the first session of *de novo* versus novel (N) learning of the five rats shown in **Figure 1**. Note the higher performance for both inbound and outbound during novel learning than *de novo* learning (****$p < 0.0001$, rank-sum tests). Also note that the below-chance performance of inbound trials during the first session of *de novo* learning is due to perseveration, consistent with previously reported behavioral patterns[1-3]. Box plots show median, 75th (box), and 90th (whiskers) percentile.

(C) Memory performance of familiar-novel animals (data points for individual animals, $n = 3$). A separate set of rats were trained on a F-N-F'-N' sequence, instead of N-F-N' shown in **Figure 1**, after *de novo* learning (**STAR Methods**). For both sets of animals, regardless of the behavioral order of novel and familiar environments, the performance in the familiar environment (blue circles) is significantly higher than that in the novel environment (gray circles; repeated-measures ANOVA with Tukey's *post hoc*, $F = 48.98$, **$p = 0.0053$, ***$p < 0.0005$), suggesting that animals were able to remember and distinguish the two environments.

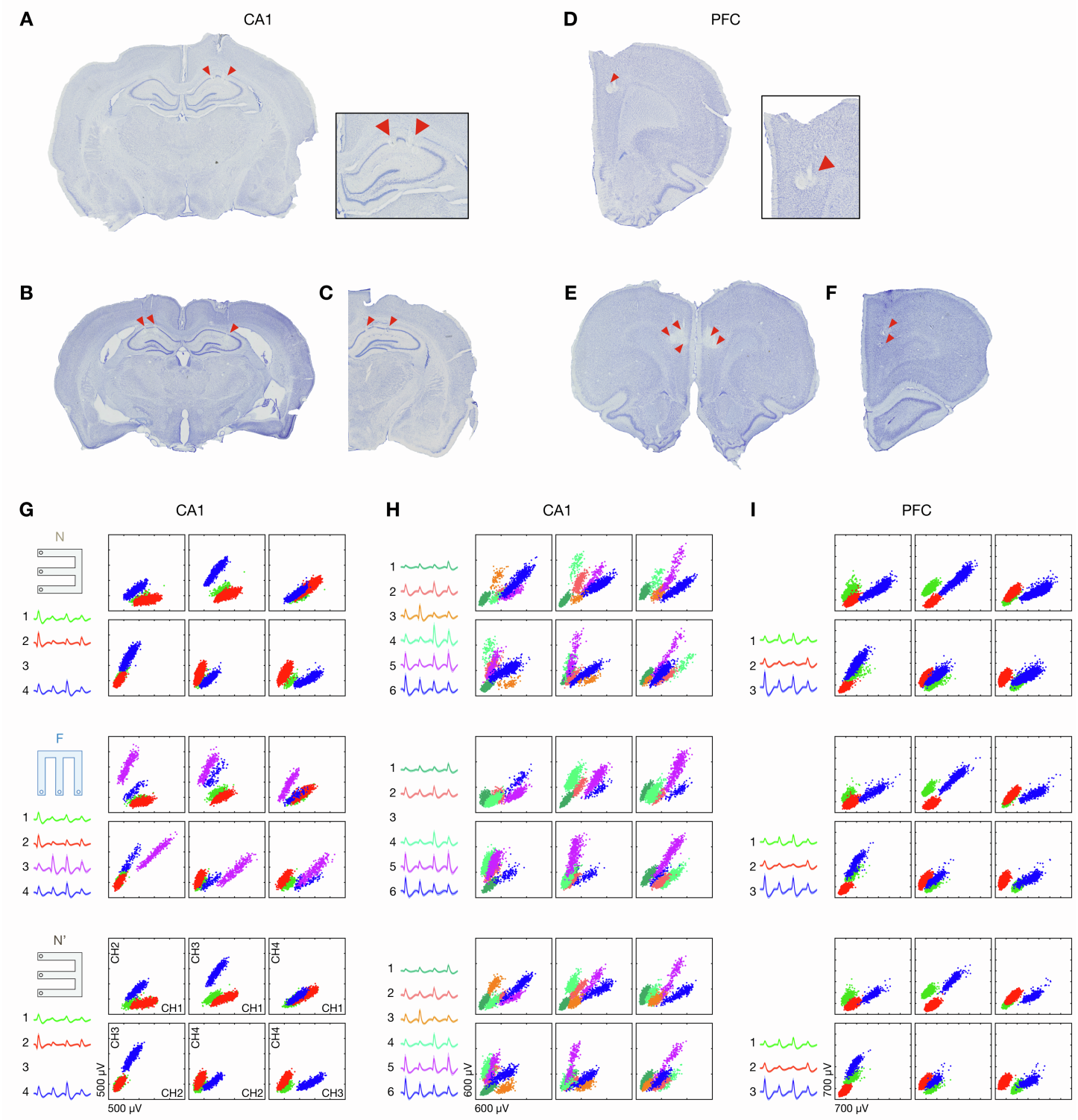

Figure S2. Electrode locations and cell clusters in different environments. Related to Figure 1.

(A-F) Representative electrode locations (arrows) in 3 rats in (**A-C**) CA1 and (**D-F**) PFC (primarily in PreLimbic cortex, with a few in rostral Anterior Cingulate Cortex as reported previously)[2,4].

(G-I) Stable cell clusters in novel and familiar environments. Spikes recorded from N, F, and N' session are shown from top to bottom. Representative cell clusters recorded from two CA1 tetrodes shown in (**G**) and (**H**), and from one PFC tetrode shown in (**I**).

Scatter plots show peak-to-trough amplitudes from two of 4 channels (CHs) of a tetrode. Each dot represents a single sampled spike, and spikes associated with each isolated single unit are shown in a different color. Spike waveforms of the example cells on 4 channels are shown on the corresponding left panels (line: mean; shading: SD). Note the stability of spike clusters and waveforms across recording sessions. Also, note that Cell 3 in (**G**) did not fire in the novel environment, and Cell 3 in (**H**) did not fire in the familiar environment.

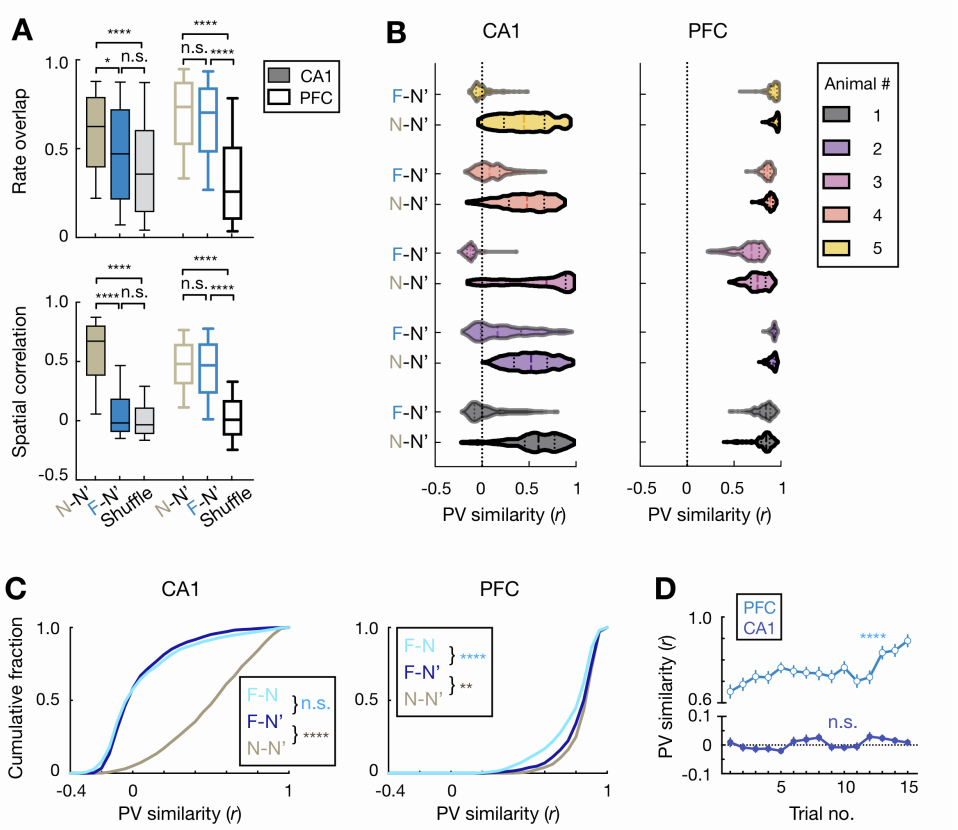

Figure S3. Remapping properties of CA1 and PFC cells. Related to Figure 2.

(A) Environment switch induces "global remapping" of CA1 cells, but not PFC cells. Changes in firing rate (i.e., rate remapping) were quantified using rate overlap (*top*), and changes in the location of firing fields (i.e., global remapping) were quantified using spatial correlation[5] (*bottom*). Note that the similarity of PFC firing across familiar-novel environments (F-N') was as large as with repeated exposures of the novel environment (N-N'; n.s., $p > 0.05$), in contrast to CA1 (*$p = 0.012$, ****$p < 0.0001$, one-way ANOVA with Tukey's *post hoc*). Shuffle: cell IDs randomly shuffled. Box plots show median, 75th (box), and 90th (whiskers) percentile.

(B) Violin plots displaying population vector (PV) similarity for each of the five animals (Animal #1-5, color-coded as in **Figure 1B**).

(C and **D)** PFC spatial representation generalized more strongly across environments with experience. **(C)** Cumulative distribution of PV similarity for F-N (light blue), F-N' (dark blue), and N-N' (gray) in CA1 (*left*) and PFC (*right*). Comparing F-N and F-N', n.s., p(CA1) = 0.093, ****p(PFC) < 0.0001; Comparing F-N' and N-N', ****p(CA1) < 0.0001, **p(PFC) = 0.0013; one-way ANOVA with Tukey's *post hoc*. **(D)** PV similarity between novel and familiar environments over trials in the novel environment. Single-trial and session-averaged rate maps were used for the novel and familiar environment, respectively. Only trials with ≥ 80% spatially-tuned cells active were included (comparing the first and last trial, n.s., p(CA1) > 0.99, ****p(PFC) < 0.0001, one-way ANOVA with Tukey's *post hoc*).

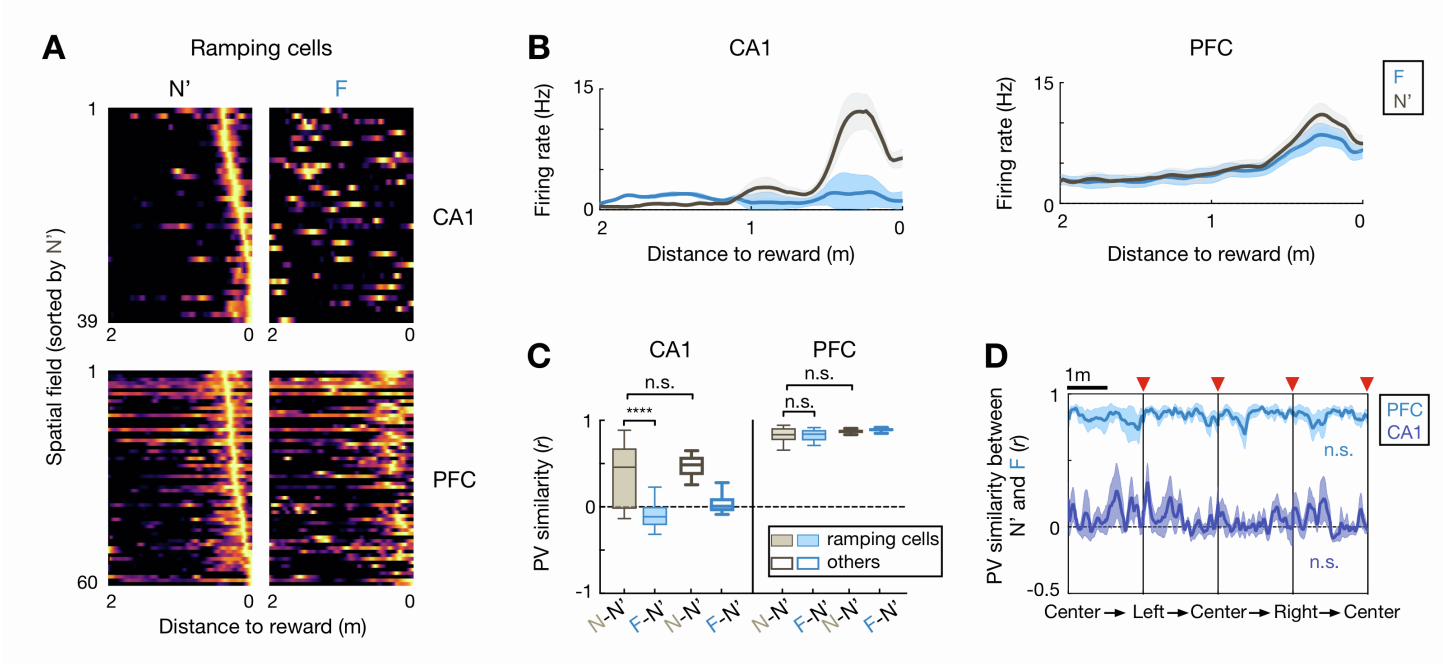

Figure S4. Reward representation in CA1 and PFC across environments. Related to Figure 2.

(A and **B)** Rate maps on 2-m long linearized trajectories of all ramping neurons (**STAR Methods**) identified in N' across environments. Rate maps of individual cells in **(A)** sorted by peak activity in N'. Rate maps in **(B)** shown mean ± SEMs. Note that ramping cells identified here (CA1: 81/495 = 16.4% cell samples; PFC: 115/636 = 18.1% cell samples across all sessions; each cell sample corresponds to data from a single cell for one trajectory type) are different from the reward coding cells reported previously, which make up fewer than 1% of all recorded cells in the hippocampus[6].

(C) PV similarity of ramping cells (filled boxes) versus other cells (hollow boxes) across novel (N-N'; gray) and familiar-novel (F-N'; blue) environments (n.s., $p = 0.05$, ****$p < 0.0001$, Kruskal-Wallis test with Dunn's *post hoc*). Box plots show median, 75th (box), and 90th (whiskers) percentile.

(D) PV similarity between the novel and familiar environment over locations across the 4 different trajectories (separated by vertical lines) in PFC (light blue) and CA1 (dark blue). The reward wells denoted on the bottom. Red arrowhead: reward location. Shading: SEM. PV similarity was consistent across locations (all p's > 0.05, Grubbs' test for outliers).

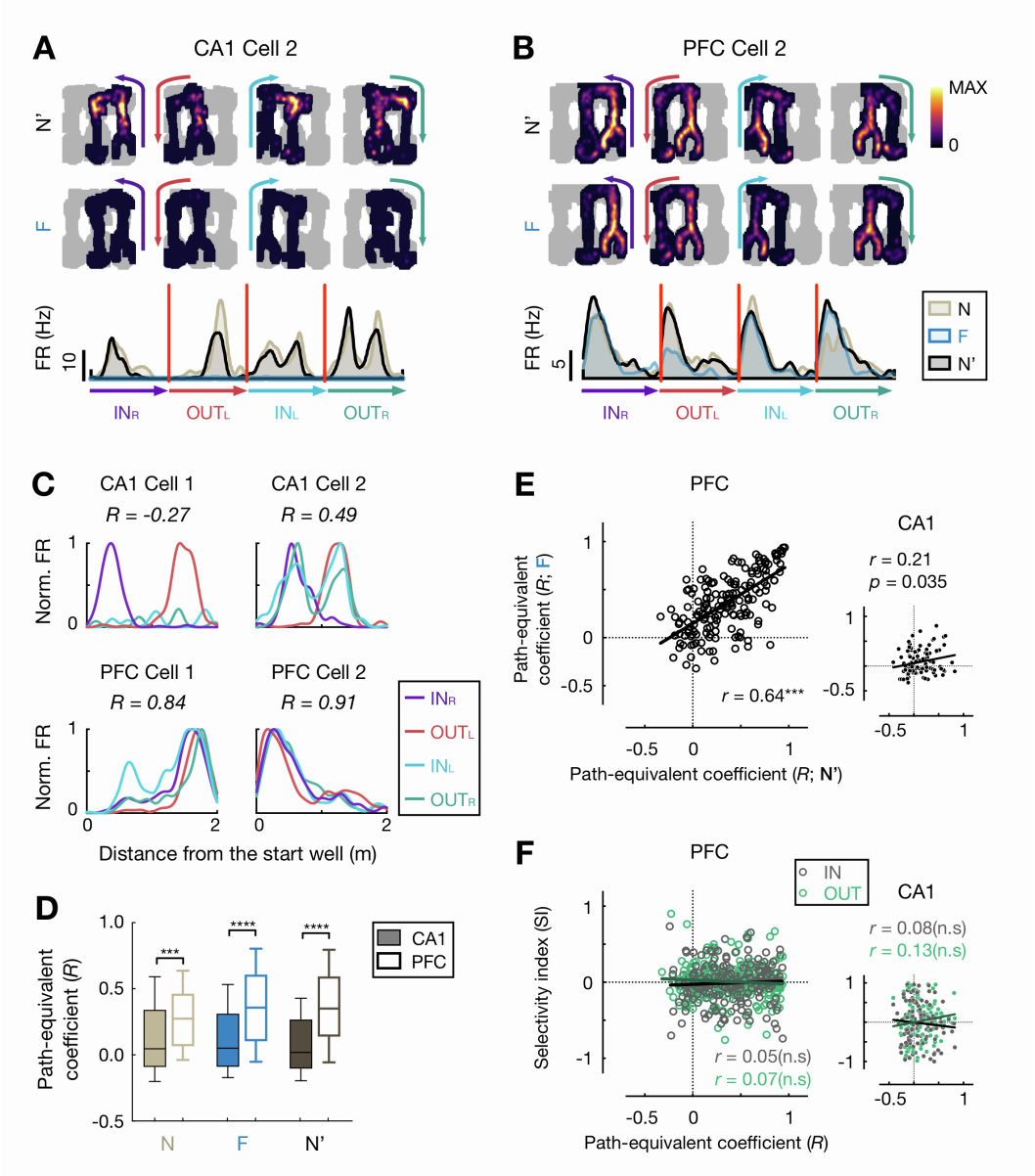

Figure S5. Robust path-equivalent representation that generalizes across trajectories and environments in PFC, but not in CA1. Related to Figure 3.

(A and **B)** Example (**A**) CA1 and (**B**) PFC cells show path-equivalent firing. Data are presented as CA1 and PFC Cell 1 in **Figures 3A** and **3B**.

(C) Normalized rate maps on different trajectory types (IN_R, OUT_L, IN_L, OUT_R, color-coded) for the example cells. Path-equivalent coefficient (*R*) denoted on top.

(D) Stronger path equivalence in PFC than CA1 (***$p = 0.0004$, ****$p < 0.0001$, $F = 25.37$, one-way ANOVA with Tukey's *post hoc*). Box plots show median, 75th (box), and 90th (whiskers) percentile.

(E) Path-equivalent coefficient is more strongly correlated between environments for PFC than CA1 (****$p < 0.0001$, $Z = 4.25$, comparing correlation coefficients; PFC, $r = 0.64$, $p = 8.43e\text{-}21$; CA1, $r = 0.21$, $p = 0.035$; Pearson correlation).

(F) Path equivalence and task-sequence selectivity are two uncorrelated measures (n.s., all p's > 0.05; Pearson correlation). IN: inbound trajectory; OUT: outbound trajectory.

Each dot is a cell sample in a given session, and lines show least-squares linear fits in (**E**) and (**F**).

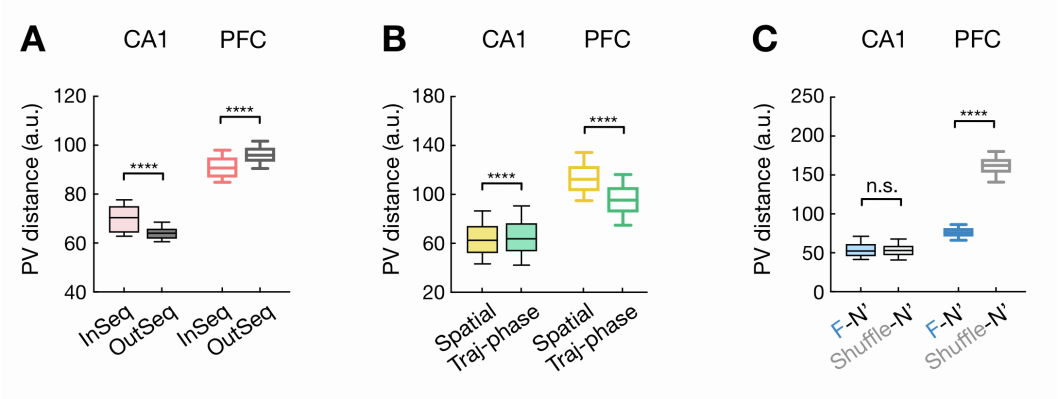

Figure S6. Distance relationship in the original high-dimensional neural space. Related to Figure 3.

(A) PV distance between pair of trajectories.

(B) PV distance between pair of neural states at same physical spatial locations or trajectory phases (traj-phase).

(C) PV distance between F and N' neural manifolds. Shuffle: cell IDs of N' activity randomly shuffled.

Data are presented as in **Figures 3H-3J**, but distance was calculated in neural state space using population vector (PV). Box plots show median, 75th (box), and 90th (whiskers) percentile. Rank-sum test, n.s., $p = 0.75$, ****$p < 0.0001$.

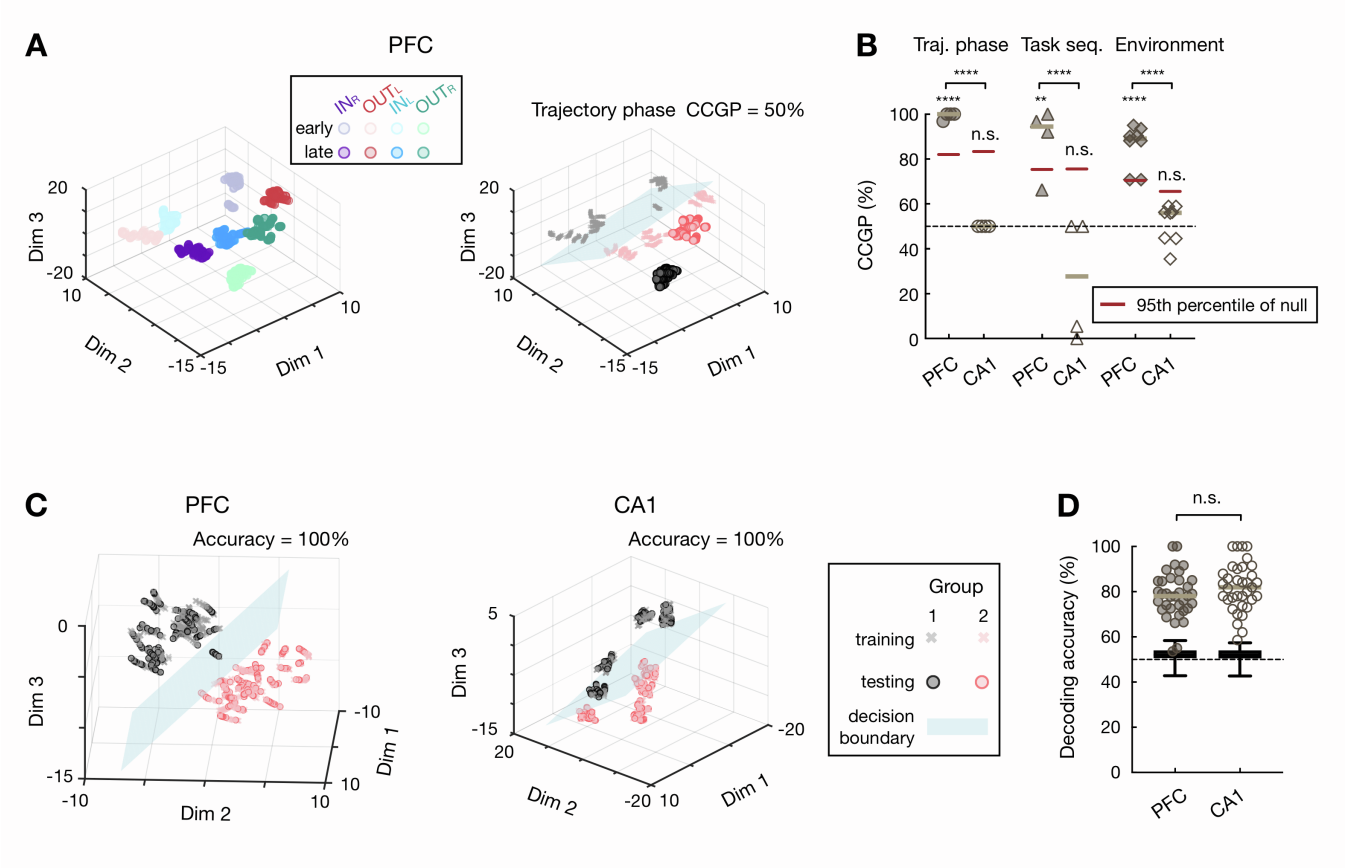

Figure S7. CCGP null models and decoding accuracy for all possible dichotomies. Related to Figure 4.

(A) An example of the geometric random model for PFC clusters. *Left*, A rotation-translation was performed independently for each cluster shown in **Figure 4A** (**STAR Methods**). *Right*, An example of CCGP for trajectory phases using the rotated clusters shown on the *left*. Data are presented as in **Figure 4C**.

(B) CCGP for trajectory phases (circles), task sequences (triangles), and environments (diamonds; horizontal lines, median) against the null-distributions of the geometric random model (red horizontal line shown the 95th percentile; n.s., $p > 0.05$, $^{**}p = 0.0026$, $^{****}p < 0.0001$). Data are presented as in **Figure 4D**.

(C) Decoding of an example dichotomy in PFC (*left*) and CA1 (*right*). Data are presented as in **Figure 4C**, but accuracy (denoted on top) was calculated using traditional cross-validation decoders, where data samples of all conditions were split into 4 groups with one group as the test data (i.e., 4-fold cross-validation; **STAR Methods**).

(D) Decoding accuracy for all 35 dichotomies (each circle is for one dichotomy). Box plots are for trial-label shuffles (n = 1,000 times), and show median, interquartile range (box), and min-max (whiskers). Note that most of the 35 dichotomies can be accurately classified in both regions, and this decoding accuracy is similar in PFC and CA1 (n.s., $p = 0.17$, rank-sum test).

References

S1. Jadhav, S.P., Kemere, C., German, P.W., and Frank, L.M. (2012). Awake hippocampal sharp-wave ripples support spatial memory. Science *336*, 1454-1458. 10.1126/science.1217230.

S2. Shin, J.D., Tang, W., and Jadhav, S.P. (2019). Dynamics of Awake Hippocampal-Prefrontal Replay for Spatial Learning and Memory-Guided Decision Making. Neuron *104*, 1110-1125 e1117. 10.1016/j.neuron.2019.09.012.

S3. Kim, S.M., and Frank, L.M. (2009). Hippocampal lesions impair rapid learning of a continuous spatial alternation task. PLoS One *4*, e5494. 10.1371/journal.pone.0005494.

S4. Tang, W., Shin, J.D., and Jadhav, S.P. (2021). Multiple time-scales of decision-making in the hippocampus and prefrontal cortex. eLife *10*. 10.7554/eLife.66227.

S5. Leutgeb, S., Leutgeb, J.K., Treves, A., Moser, M.B., and Moser, E.I. (2004). Distinct ensemble codes in hippocampal areas CA3 and CA1. Science *305*, 1295-1298. 10.1126/science.1100265.

S6. Gauthier, J.L., and Tank, D.W. (2018). A Dedicated Population for Reward Coding in the Hippocampus. Neuron *99*, 179-193 e177. 10.1016/j.neuron.2018.06.008.